Supporting Information: Supramolecular Chirality Synchronization in Thin Films of Plasmonic Nanocomposites

*Piotr Szustakiewicz, Natalia Kowalska, Dorota Grzelak, Tetsuya Narushima, Monika Góra, Maciej Bagiński, Damian Pociecha, Hiromi Okamoto, Luis M. Liz-Marzán, Wiktor Lewandowski**

SUPPLEMENTARY NOTES

Note S1: Linear dichroism in HNF@Au@L samples.

In most cases of purely organic liquid crystalline helical nanofilaments, optical activity can be detected by comparing images of a sample placed between polarizers crossed at angle 90°-n and 90°+n (where n ≈ 5-10°). In our case, by depositing 24 nm gold nanoparticles as a line with close-packing (distances < 4 nm) along the direction of the filaments, we introduced strong linear dichroism to our sample. Note the characteristic behavior of small domains with radial orientation (filaments growing evenly from single crystallization point outwards) in different polarizers setup (**Figure S11**). This prompted us to use LCP and RCP to illuminate the sample and directly compare the difference in absorption.

Note S2: CD imaging microscopy methods

Two techniques of CD imaging microscopy were used here.

1) scanning CD microscope with discretely modulated circularly polarized light (DMCPL) developed by T. Narushima and H. Okamoto,[76] which uses rapid, cyclic changes of handedness of circular polarization through a custom-made setup. ΔExt value in ellipticity units was calibrated with a standard sample with known absorbance in the CD microscope with DMCPL. The mean g-factor for a single domain ($g \approx 7.5x10^{-4}$) was calculated based on our experimental micro-CD measurement results.

Note that the CD microscopy image in **Figure 3d** shows tiny, opposite contrast spots within each domain. As the source of this effect, HNFs with opposite handedness can be considered. However, since the amount of HNFs with opposite handedness was limited, based on statistical analysis from our AFM observations of the Au@HNFs in Figure S14, the source of tiny spots could not be attributed only to the HNFs with opposite handedness. Ideally, the bare substrate part should be observed as a uniform black-colored region, where it satisfies that ΔExt = 0. Since the signal level of local CD (max. ~130 mdeg in ellipticity units), is not very large compared to the detection limit of our CD microscope (~20 mdeg in ellipticity units (0.0006 in O.D. units)), weak fluctuations with both positive and negative CD signal are observed in the substrate part, which may originate, e.g. from microscale-defects such as bumps on the substrate surface (e.g., Figure 5 in ref. 76).

2) Less precise but faster POM-CD approach devised in this work, which simply compares microscopic images obtained under RCP and LCP illumination using a traditional polarization optical microscope. To change the rotation of circularly polarized light we manually rotate the quarter wave plate in relation to linear polarizer in between the image acquisitions. For each polarization, from 3 to 10 images are obtained using a commercial digital camera at the same wavelengths (523±20 nm). Then, all images for each polarization are converted to 2D intensity maps and averaged (**Figure S14**a, b). To obtain a CD-intensity map, the difference between

averaged images for two polarizations is calculated (**Figure S14**c). To confirm the ability to measure CD-signal by this method, a sample fragment was mapped at different orientations (**Figure S14**d-f), giving the same, consistent signal for each visible domain. It is crucial for the sample to maintain its position during the whole process of image acquisition and wave plate rotation, otherwise the calculated image difference will show strong differences at the edges of all domains (**Figure S14**d). The time required to obtain qualitative results is equal to the time needed to take pictures of sample under two polarizations. In the typical setup, using 20x magnifying lens, this roughly translates to 1.25 minute/mm^2 of sample.

SUPPLEMENTARY FIGURES

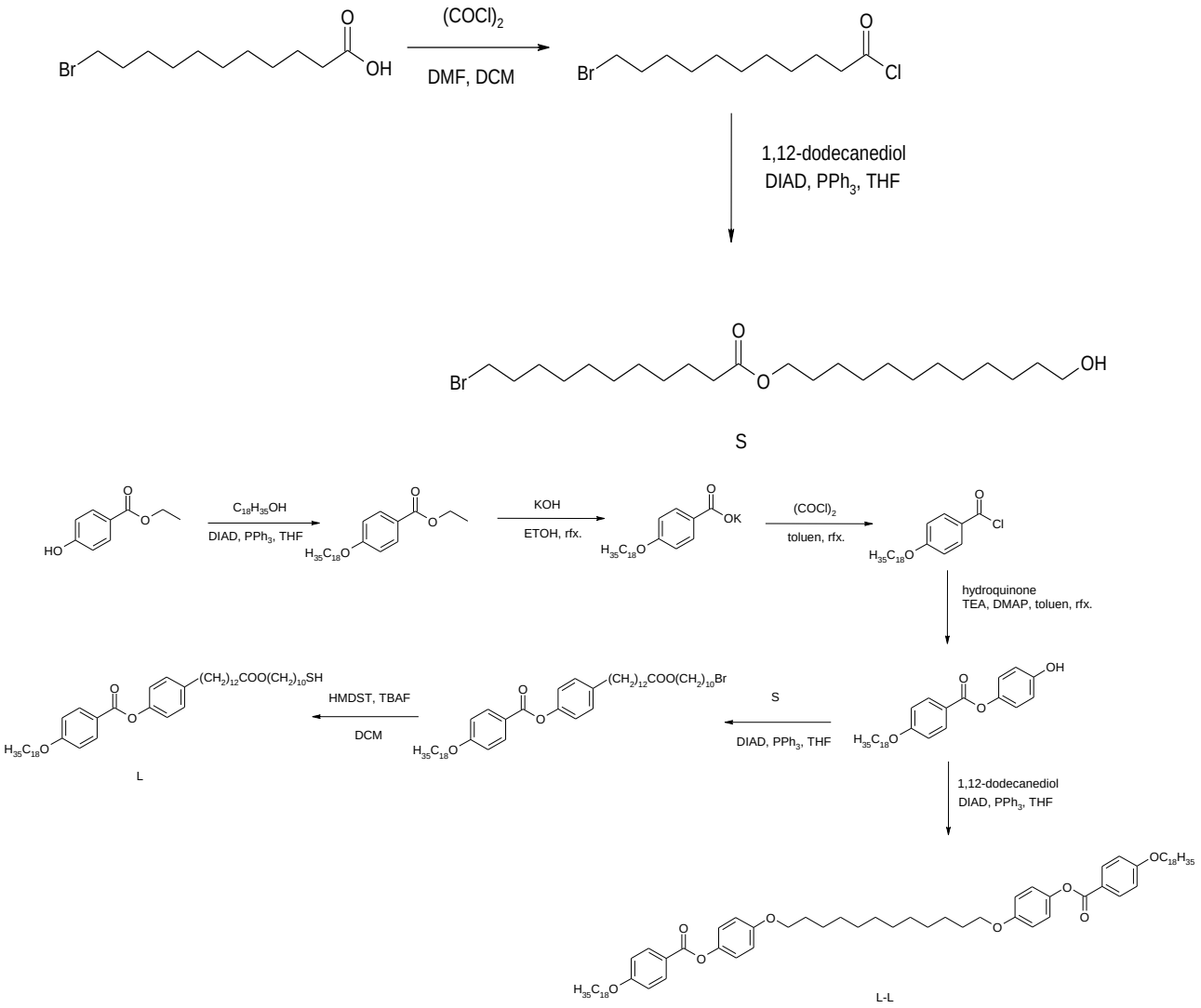

Figure S1. Synthetic route for the preparation of L and L-L compounds. Abbreviations: DMF- N,N-dimethylformamide; DCM- dichloromethane; DIAD- diisopropyl azodicarboxylate; PPh_3- triethylphosphine; THF- tetrahydrofuran; TEA- trimethylamine; DMAP- 4-dimethylaminopyridine; HMDST- bis(trimethylsilyl)sulfide; TBAF- tetrabutyloammonium fluoride.

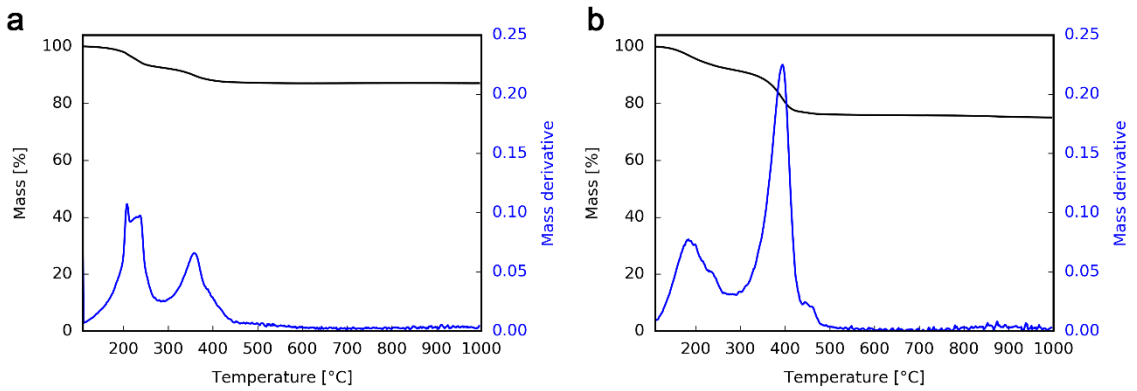

Figure S2. Thermogravimetric analysis of functionalized nanoparticles. (a) % mass (black line) and % mass derivative (blue line) for Au@L material, used to prepare HNF@Au@L. (b) % mass (black line) and % mass derivative (blue line) for Au decahedral nanoparticles functionalized solely with ligand L. Based on the results shown in (b), the ratio of mass loss in temperatures below and above 270 °C was calculated for removal of L ligands. This ratio was used to extract mass loss below 270 °C in (a) which does not come from the removal of L (i.e. it comes from the removal of DDT, which usually occurs below 250 °C[S1]). The L:DDT molar ratio was estimated as 1:2 in the organic shell of Au@L nanoparticles.

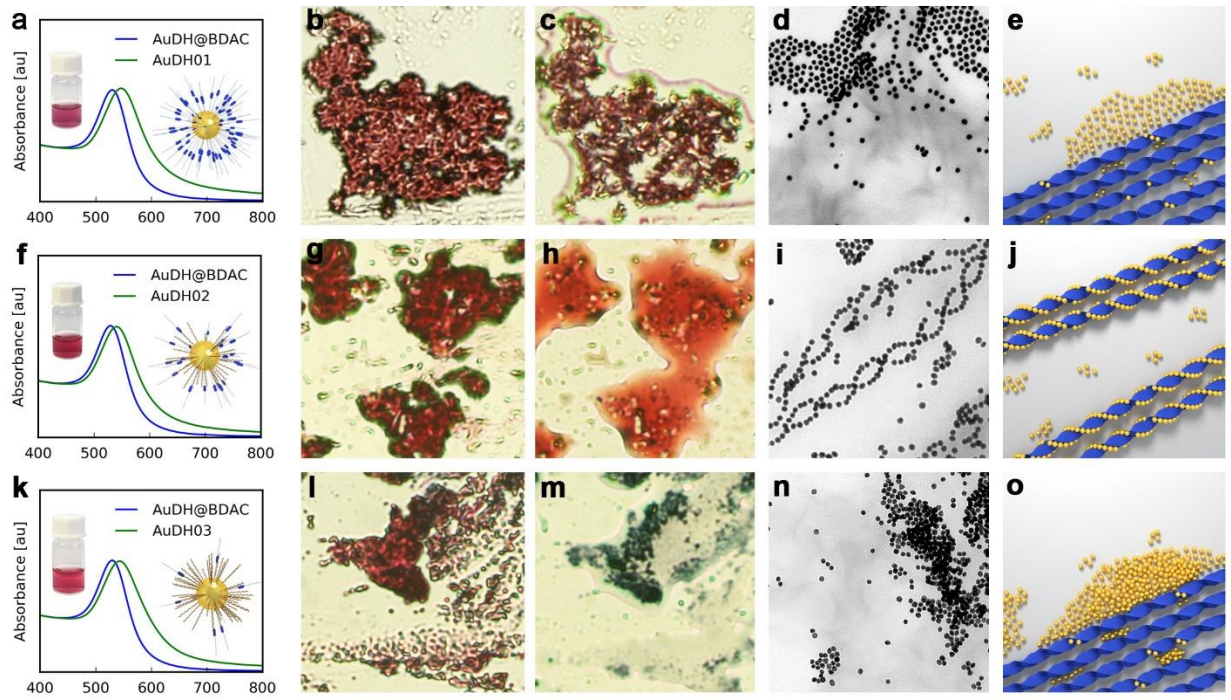

Figure S3. Optimization of the process for obtaining HNF@Au@L. (a) Thermogravimetric analysis of nanoparticles Stability of modified NP was confirmed using UV-Vis spectroscopy. Panels a, f, k show UV-Vis spectra before and after ligand exchange, carried out in various molar ratios of Au^0 to L to DDT – 1:1:0 (a), 1:1:1 (b), 1:0.5:1.5 (k). Before the heating – cooling cycle, the stability of NP in dimer matrix at room temperature (b, g, l) and 140 °C (c, h, m) was checked. After the heating – cooling cycle the structure of obtained HNF@Au@L was confirmed (d, i, n) – only a molar ratio 1:1:1 allowed for helical self – assembly.

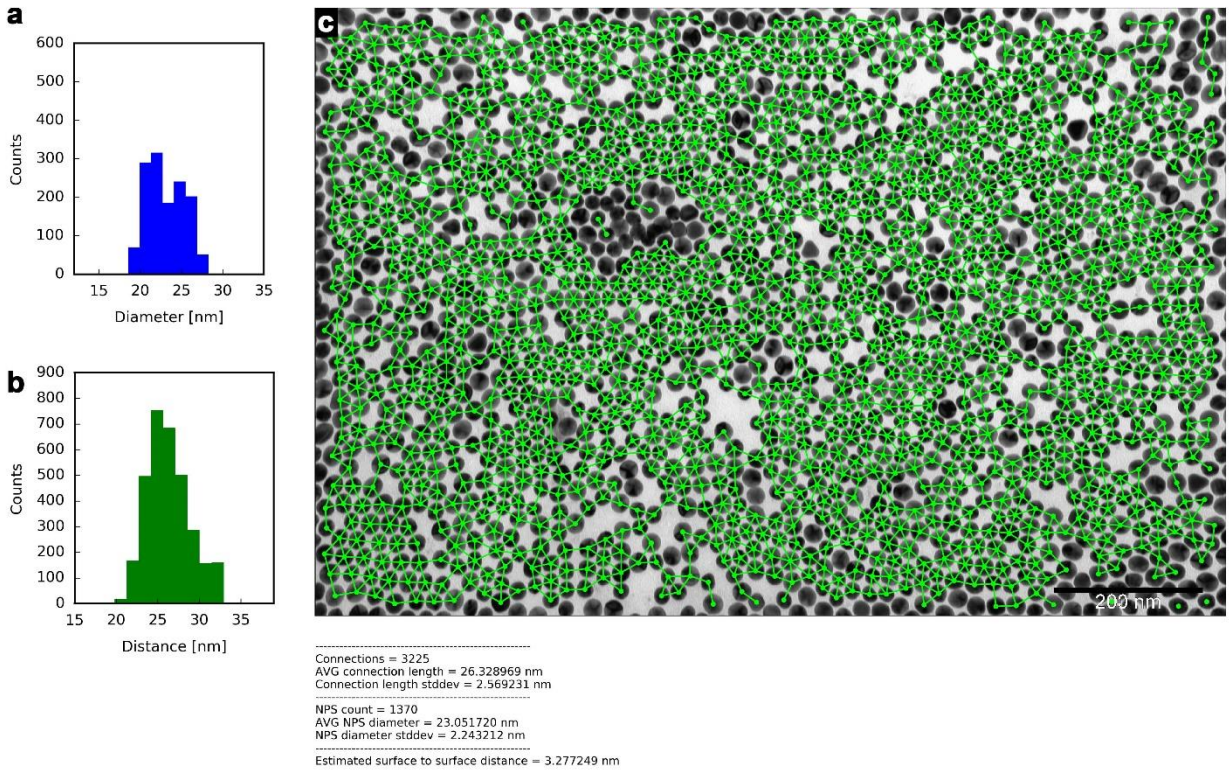

Figure S4. Histogram of nanoparticles diameter (a) after functionalization with L and histogram of (center-to-center) distances (b) between neighboring nanoparticles as measured from the TEM image (c).

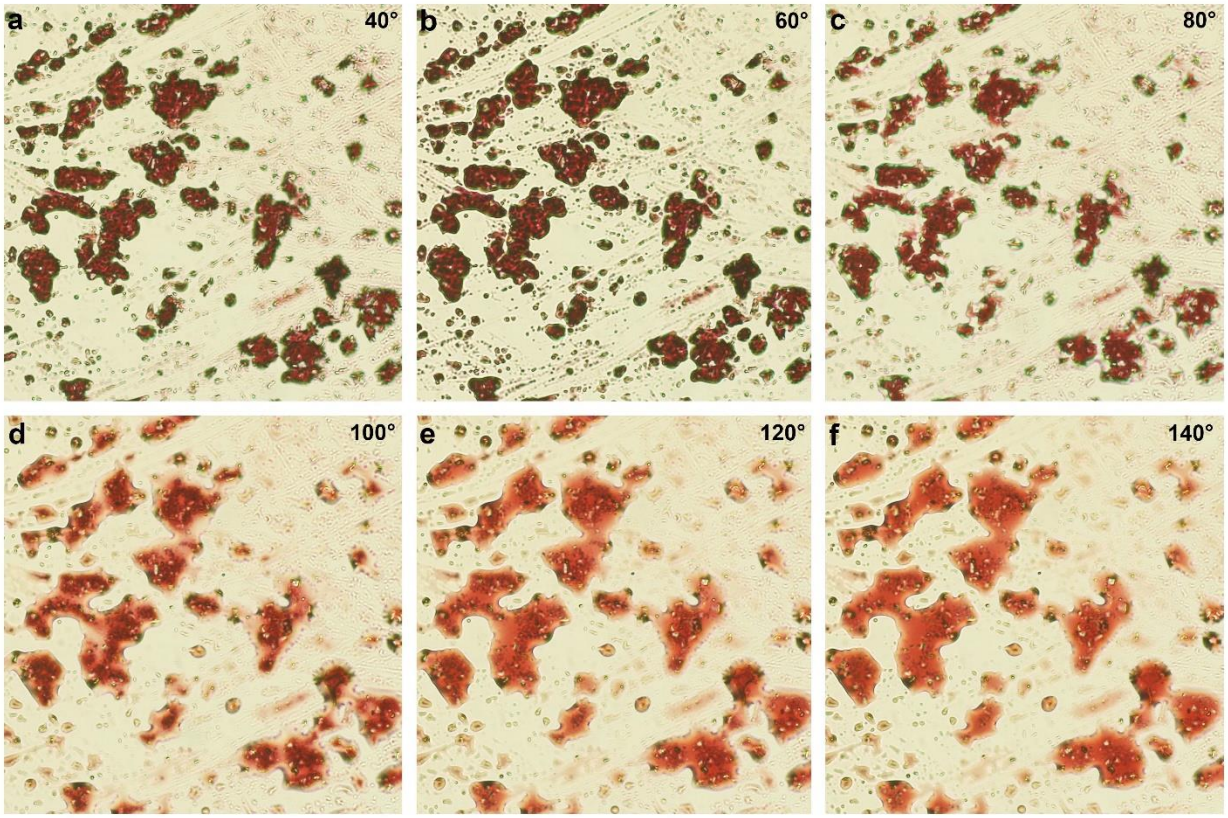

Figure S5. Optical images of sample fragments during the heating procedure, showing the melting of Au@L NPs in L-L dispersion. Although L-L melting occurs at around 90 °C, the sample was heated to higher temperatures to ensure an even dispersion of nanoparticles. Note that in 100 °C (d), the NPs aggregates are still clearly visible despite the L-L matrix being an isotropic liquid; experimentally we found that heating the samples to 140 °C (f) ensures the highest yield of HNF@Au@L assemblies during cooling.

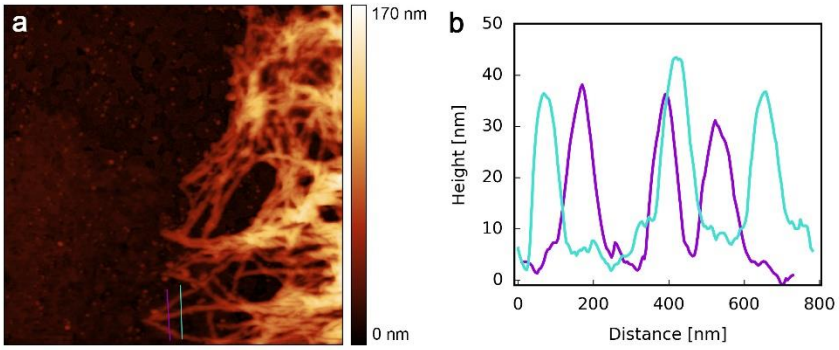

Figure S6. AFM height map o sample analyzed prior to SEM measurements along with the elevation profiles marked by violet and green lines.

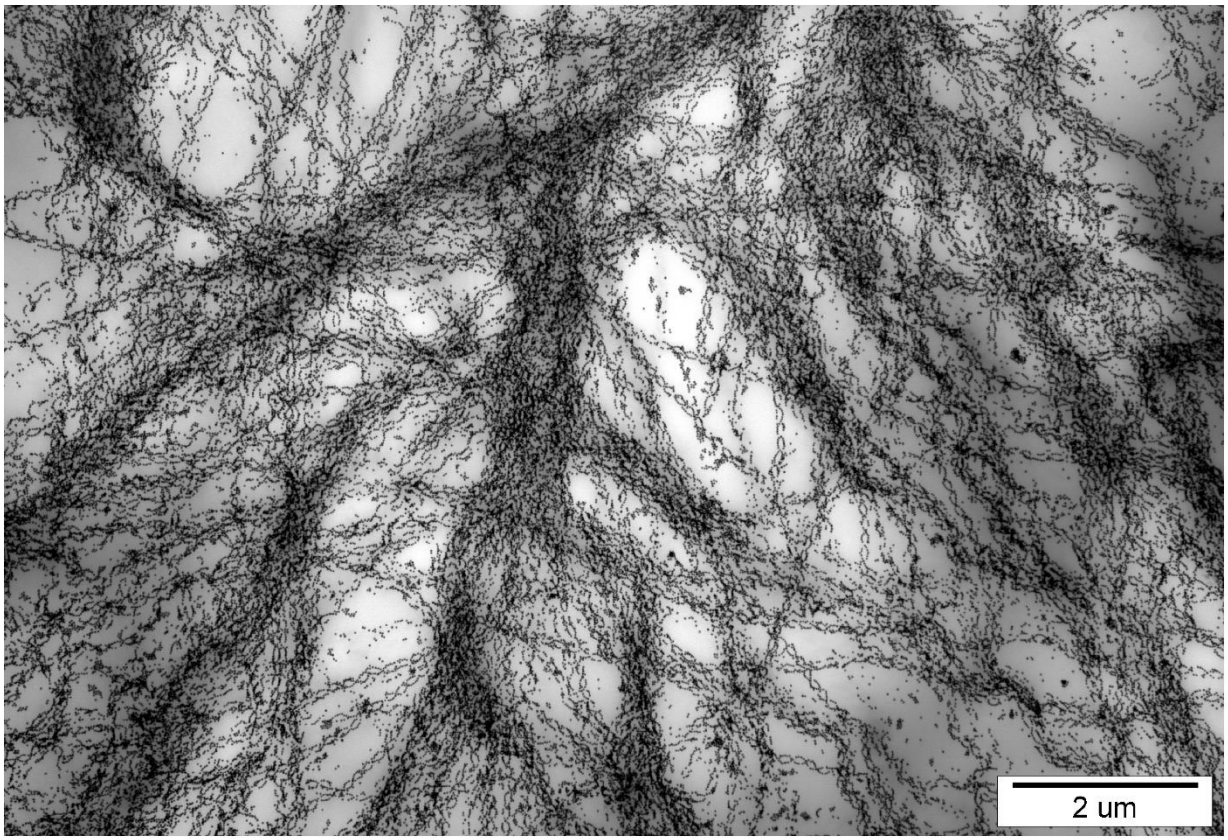

Figure S7. TEM image of HNF@Au@L.

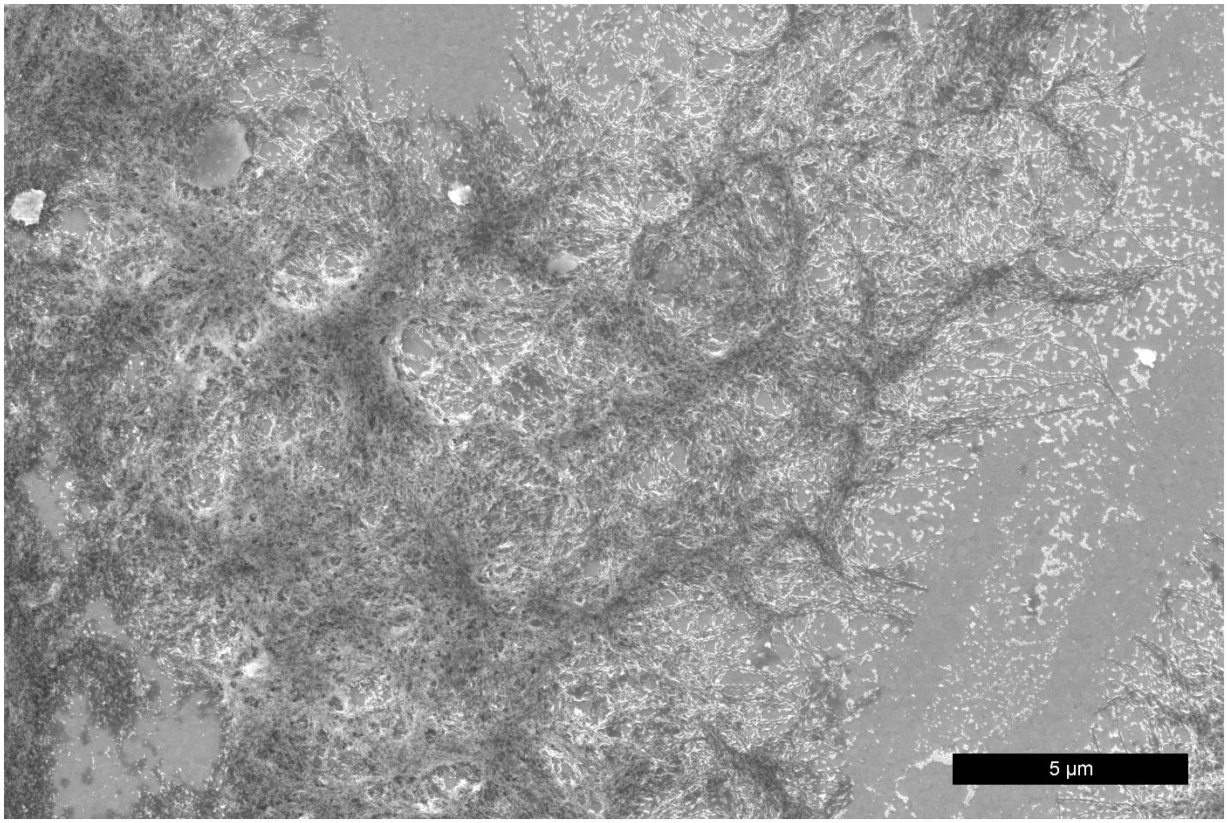

Figure S8. SEM image of an HNF@Au@L domain.

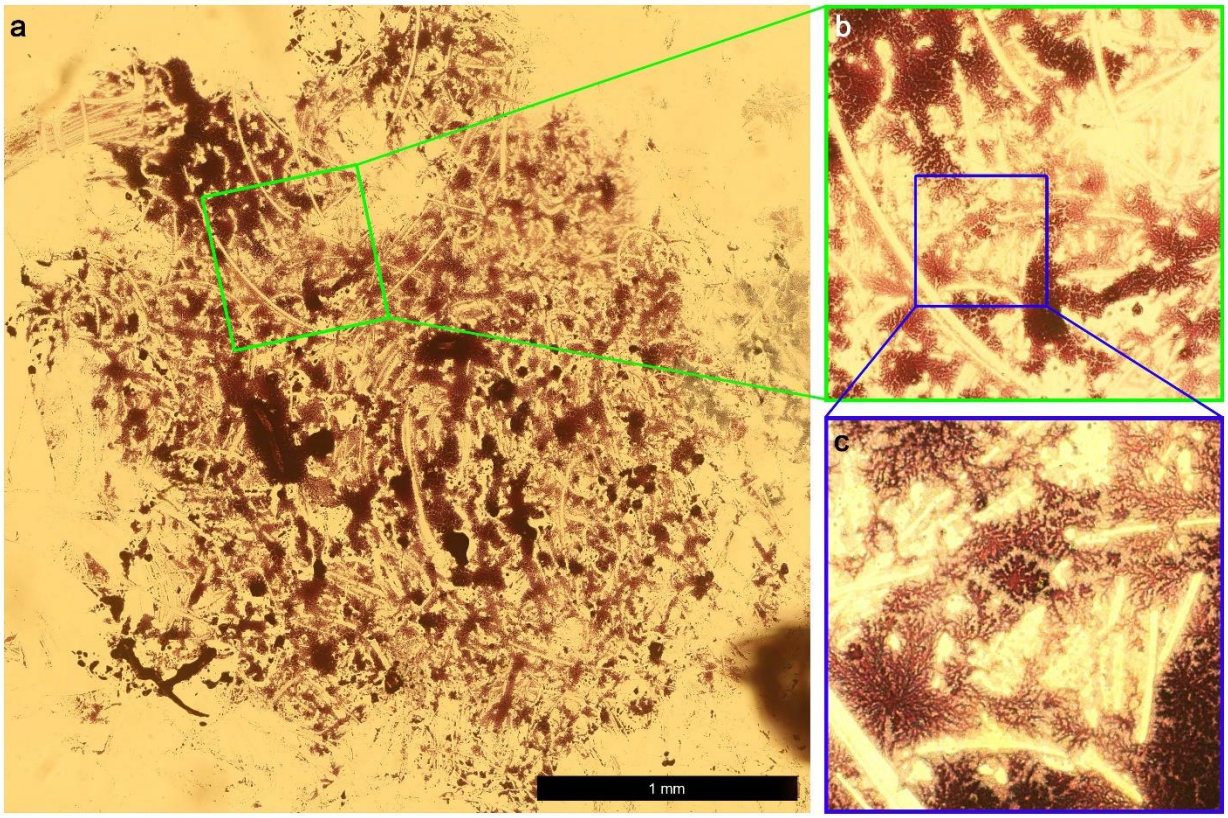

Figure S9. Optical microscope image of entire area of one of the HNF@Au@L sample before chiral discrimination.

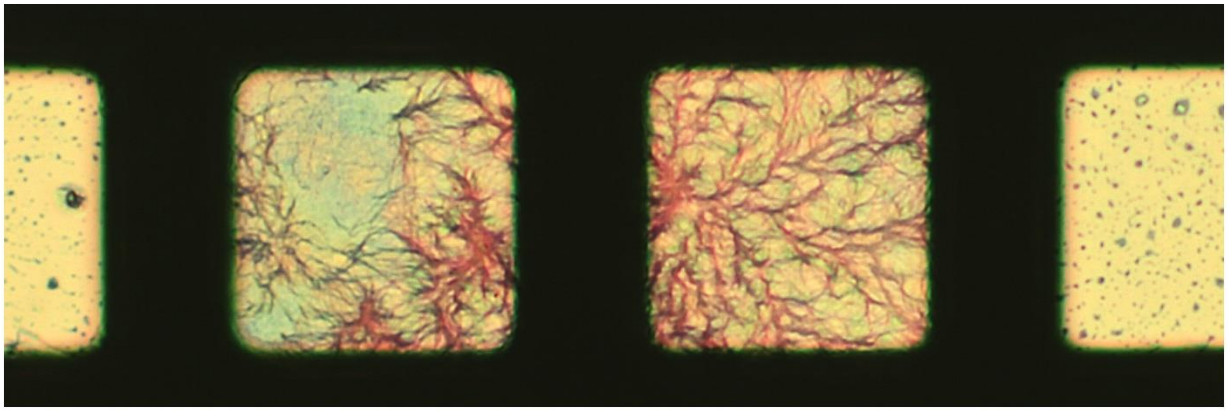

Figure S10. The optical microscopy image showing a larger domain, covering entire grid hole (part of this image is displayed in Figure 2a, in the main text).

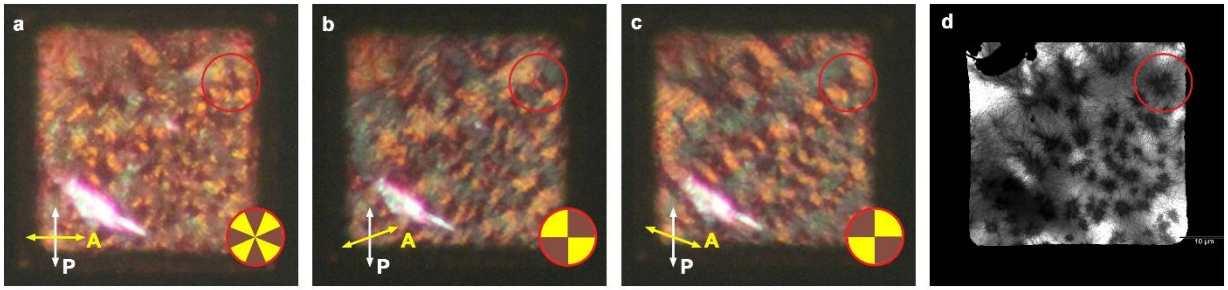

Figure S11. Polarization optical microscopy images showing linear dichroism of HNF@Au@L filaments. (a) Image of a sample between two crossed polarizers at 90°. Note the characteristic pattern marked by the top red circle and graphically represented in the bottom right corner. Note the change of pattern as we change the polarizer angles to 85° (b) and 95° (c). TEM image (d) of the same area confirms the presence of HNF@Au@L domains.

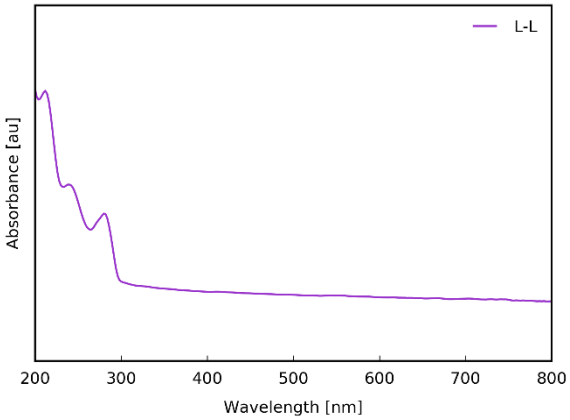

Figure S12. UV-VIS spectrum of L-L matrix in solid state showing no absorbance peaks in regions, where CD was measured.

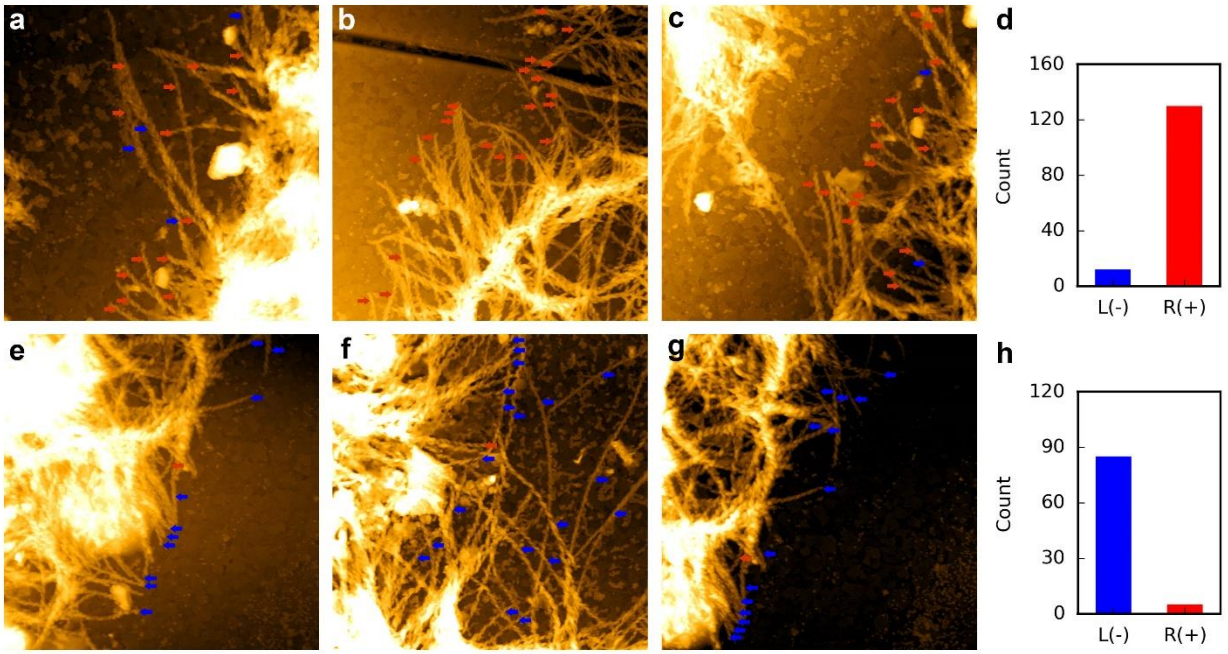

Figure S13. 2D AFM elevation profiles of HNF@Au@L domains. Panels a, b and c shows selected maps for domain with negative ΔExt signal during DMCPL signal measurements (**Figure 3**c), while panels d, e and f corresponds to maps of positive ΔExt signal domains. Single helical filaments with right- and left- handedness are marked with red and blue dots respectively. Note that right-handed filaments are predominant for domains with positive ΔExt signal while for negative ΔExt signal domain left-handed filaments are a majority. Statistical analysis using more AFM maps is shown on panels d and h.

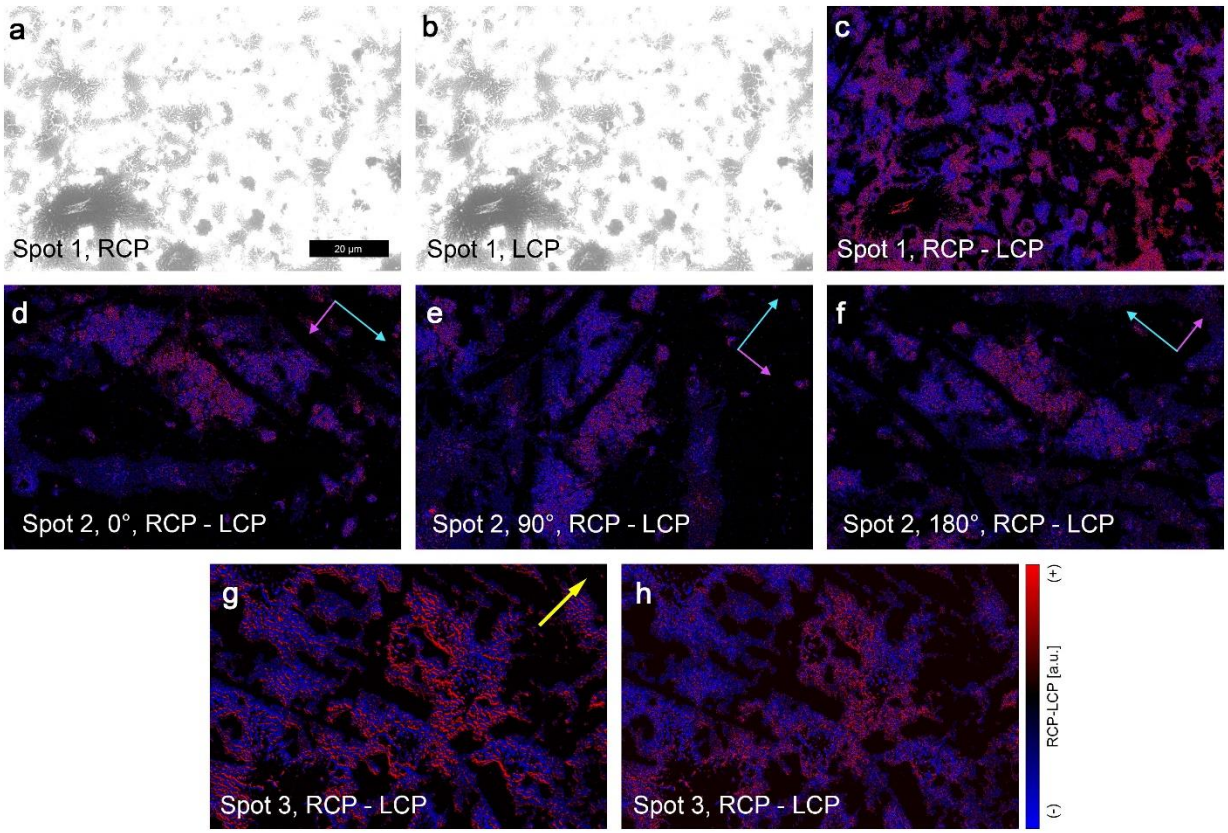

Figure S14. POM-CD method. (a-b) Data obtained by averaging 5 images of the sample illuminated by RCP (a) and LCP (b), displayed as a grayscale intensity maps. Visual inspection of both maps does not reveal any differences, however by subtracting one map from the other we obtain light transmission difference map (c), which grants the ability to distinguish HNF@Au@L domains by circular dichroism. Note the 'hole' in the bottom-left aggregate on (c), which is caused by the large thickness of this aggregate. (d-f) Comparison of CD-signal map of different area taken at a different sample orientation (0°, 90° and 180° respectively), note the domain signal consistency. Comparison of the results if the sample was slightly moved during image acquisition (g), a yellow arrow shows the direction of the drift, and the CD map of the same area with images obtained without drift (h).

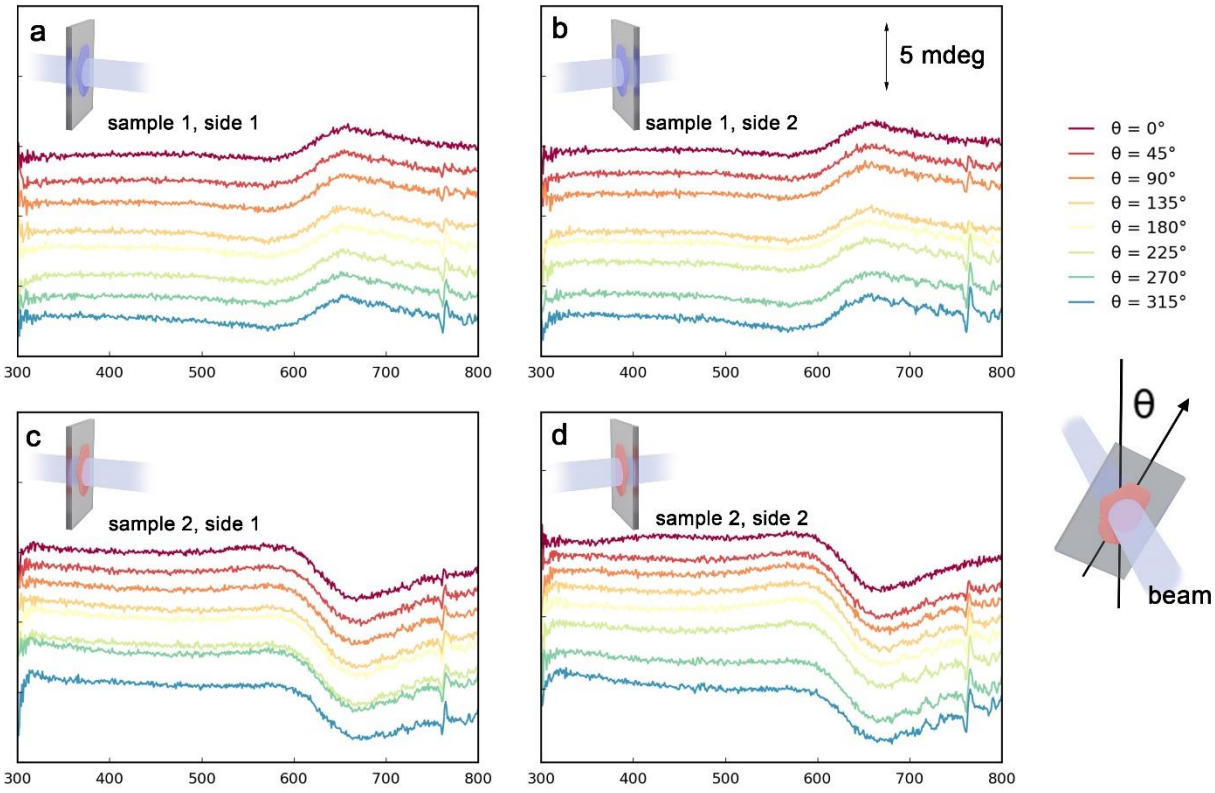

Figure S15. (a) Circular dichroism spectra of HNF@Au@L samples rotated along the probing beam axis for 0°, 45°, 90°, 135°, 180°, 225°, 270° and 315°, (b) the same sets of measurements after rotating the sample 180° along the axis perpendicular to the probing beam. (c, d) Results corresponding to panels a and b, acquired for a sample with the opposite handedness of domains.

S1. Lewandowski, W.; Constantin, D.; Walicka, K.; Pociecha, D.; Mieczkowski, J.; Górecka, E. Smectic Mesophases of Functionalized Silver and Gold Nanoparticles with Anisotropic Plasmonic Properties. *Chem. Commun.* **2013**, *49*, 7845.